Pharmaceutical Research, Vol. 23, No. 7, July 2006 (© 2006)
DOI: 10.1007/s11095-006-0278-6

Research Paper

Lipopolyamine-Mediated Single Nanoparticle Formation of Calf Thymus DNA Analyzed by Fluorescence Correlation Spectroscopy

Noppadon Adjimatera,[1] Teresa Kral,[2,3] Martin Hof,[2] and Ian S. Blagbrough[1,4]

Received December 21, 2005; accepted February 27, 2006

Purpose. The aim of this study is to analyze linear calf thymus DNA (ct DNA) nanoparticle formation with N^4,N^9-dioleoylspermine and N^1-cholesteryl spermine carbamate.
Methods. Fluorescence correlation spectroscopy (FCS) was used to determine the quality of ct DNA condensed by lipopolyamines. ct DNA was prelabeled with PicoGreen® (PG) to allow fluorescence intensity fluctuation measurement and analysis.
Results. N^4,N^9-Dioleoylspermine efficiently condensed ct DNA into point-like molecules with diffusion coefficient (D) = 1.8×10^{-12} m^2/s and particle number (PN) = 0.7 [at ammonium/phosphate (N/P) charge ratio=1.0–1.5]. The determined PN values are close to the theoretical value of 0.6, providing evidence that the DNA conformation has been fully transformed, and thus a single nanoparticle has been detected. N^1-Cholesteryl spermine carbamate showed (slightly) poorer DNA condensation efficiency, even at higher N/P ratios (N/P = 1.5–2.5) with $D = 1.3 \times 10^{-12}$ m^2/s and PN value of 5.2. N^4,N^9-Dioleoylspermine is a more efficient DNA-condensing agent than N^1-cholesteryl spermine carbamate.
Conclusions. FCS measurement using PG as the probe is a novel analytical method to detect single nanoparticles of condensed DNA in nonviral gene therapy formulation studies.

KEY WORDS: N^1-cholesteryl spermine carbamate; N^4,N^9-dioleoyl spermine; fluorescence correlation spectroscopy; lipopolyamines; single nanoparticle.

INTRODUCTION

Nonviral gene therapy (NVGT), a new treatment strategy using (synthetic) chemical-based vectors, has been employed to treat genetic disorders as well as other nongenetic diseases, especially cancer. The focus on nonviral vectors for DNA delivery has shown a remarkable increase worldwide (1–4). Unlike conventional chemical-based medicines, the therapeutic DNA in gene therapy is used as (a prodrug for) the pharmacologically active ingredient and formulated appropriately for administration to patients' cells, aiming for desired gene expression to therapeutic protein in patients. The success rate in gene therapy still drags behind expectations due to the lack of safe and efficient gene delivery (vector) formulations (5–7). A prerequisite step in gene delivery is DNA nanoparticle formation, which allows the reduction and charge neutralization of DNA. This DNA condensation process is initiated by the interaction of positively charged NVGT vectors with negatively charged phosphate groups on the DNA double helix (8–12), leading to the formation of a DNA nanoparticle by means of a lipopolyamine vector and self-assembly. After nanoparticle formation they must enter cells, most likely by endocytosis, escape from the endosome–lysosomal system, and gain entry to the nucleus where gene expression takes place.

The lipid–polyamine conjugates (lipopolyamines) are efficient gene delivery vectors, achieving high DNA packaging and improved *in vivo* gene delivery results. These molecules incorporate a lipophilic moiety (mainly long-chain hydrocarbon or steroidal lipids) and positively charged amine group(s), such as spermidine or spermine (5,13–16). DNA binding by lipopolyamine vectors plays an important role in gene delivery success. DNA condensation affords nanoparticles

[1] Department of Pharmacy and Pharmacology, University of Bath, Bath, BA2 7AY UK.
[2] J. Heyrovský Institute of Physical Chemistry, Academy of Sciences of the Czech Republic, Dolejškova 3, 182 23 Prague 8, Czech Republic.
[3] Department of Physics and Biophysics, Agricultural University, Norwida 25, 50-375 Wrocław, Poland.
[4] To whom correspondence should be addressed. (e-mail: prsisb@bath.ac.uk)

ABBREVIATIONS: A, correction factor; AF488, Alexa Fluor-488; C, molarity; CR, count rate; ct DNA, calf thymus DNA; D, diffusion coefficient; DNase, nuclease; dsDNA, double-stranded DNA; D_w, diffusion coefficient in water; EthBr, ethidium bromide; FCS, fluorescence correlation spectroscopy; $G(\tau)$, autocorrelation function; HEPES, 4-(2-hydroxyethyl)-1-piperazine-ethanesulfonic acid; I, fluorescence intensity signal; k_B, Boltzmann constant; M, molecular mass; N/P, ammonium/phosphate ratio; N_A, Avogadro's number; NPC, nuclear pore complex; NVGT, nonviral gene therapy; PG, PicoGreen®; PN, particle number; r_h, hydrodynamic radius; R6G, Rhodamine-6G; SMS, single-molecule spectroscopy; ssDNA, single-stranded DNA; T, triplet fraction; T_c, thermodynamic temperature; V, confocal volume; η, dynamic viscosity; τ, correlation time; τ_{tr}, triplet decay time; τ_D, diffusion time; ω_1, lateral radii of detection volume; ω_2, axial radii of detection volume

with the appropriate size to enter cells and gives protection from nuclease (DNase), important properties when considering serum stability for *in vivo* applications. Disassociation of DNA from the vector at the right time is crucial, possibly after escaping from the endosome and just before reaching, or immediately after entering, the nucleus. However, the mechanisms of association and dissociation between lipopolyamines and DNA are still not well understood (5,13–18). The specifics of the mechanisms of gene delivery using NVGT, at the level of molecular pharmaceutics, follows: DNA typically self-assembles with the lipopolyamine to form a nanoparticle by charge neutralization. The DNA complex can enter cells mainly by endocytosis. DNA complexes are encapsulated in the endosomal vesicles, which are susceptible to enzymatic degradation. These particles must be released from the endosomes before the lysosome is fused to the endosomes. Translocation into the nucleus involves the transportation of DNA through the nuclear pore complex (NPC) (or during mitosis). The last step of gene delivery is successful gene expression.

Fluorescence correlation spectroscopy (FCS) is a new technique to study molecular interactions based on fluorescence, combining steady-state fluorescence spectroscopy and confocal microscopy (19,20). In conventional fluorescence spectroscopy, a relatively large volume of sample is illuminated by an excitation laser. The average fluorescence intensity is recorded with high background noise, leading to limitation in resolution and sensitivity. With the confocal microscopy technology, the (very small) sample volume (the "confocal volume," V, of about 1 fL) is defined by a focused laser beam and a confocal pinhole. This volume is small enough to host only one molecule at detectable practical concentrations; hence, FCS is also regarded as "single-molecule spectroscopy" (SMS) (21,22). The fluorescence is collected with a high-aperture microscope objective and monitored by a sensitive single-photon counting detector. The measured fluorescence from single molecules fluctuates with time, and these temporal fluctuations are autocorrelated. The normalized fluorescence fluctuation autocorrelation function provides two types of information: The magnitude is inversely related to the average number of observed fluorescent molecules, and the rate and shape of the temporal decay reflects the dynamic properties of the observed molecules. This autocorrelation function allows faster and slower diffusing particles to be differentiated (19–25). The FCS technique has been used to study dynamic processes, on the molecular scale, including DNA nanoparticle formation in drug delivery (26–28). There were also some studies on oligonucleotide–lipid complex using FCS, in addition to polynucleotide (DNA) (29–34). This study is aimed at the analysis of (single) DNA nanoparticle formation employing two lipopolyamines, N^4,N^9-dioleoylspermine and N^1-cholesteryl spermine carbamate, and linear calf thymus DNA (ct DNA).

MATERIALS AND METHODS

Materials

PicoGreen® (PG), Rhodamine-6G (R6G), and Alexa Fluor-488 (AF488) were obtained from Molecular Probes (Eugene, OR, USA). Ethidium bromide (EthBr), ct DNA (minimum size 13 kbp), and chemicals used to prepare 4-(2-hydroxyethyl)-1-piperazine-ethanesulfonic acid (HEPES) buffers were purchased from Sigma-Aldrich (Poole, Dorset, UK). HEPES buffer was composed of 2 mM HEPES, 20 mM NaCl, 10 μM EDTA, and MilliQ water. The final pH was adjusted to 7.4 with aq NaOH solution. The HEPES buffer was filtered through a 0.45-μm membrane before use. N^4,N^9-Dioleoylspermine and N^1-cholesteryl spermine carbamate were synthesized as we have previously reported (35,36).

PicoGreen Concentration Determination

PG is patented and its concentration was not provided by Molecular Probes. Diluted PG solution absorbance was measured with a UV spectrophotometer at 500 nm. The molar concentration was then calculated by using the molar absorptivity from the literature (70,000 M^{-1} cm^{-1} at 500 nm) (37). The PG solution supplied by Molecular Probes was found to be 220 μM, and therefore its 1/200 dilution (i.e., at the recommended dilution by the manufacturer) is 1.1 μM.

DNA Sample Preparation and Quantification

ct DNA sample was dissolved in HEPES buffer and stored at −80°C. For quantification of DNA, a 5-μL sample was diluted to 1 mL with water and the UV absorbance was measured at 260 and 280 nm on a GeneQuant II spectrophotometer. TE buffer (5 μL diluted to 1 mL in water) was used as a standard reference. The A260/A280 ratio was calculated to analyze the purity of the DNA (38,39).

ConfoCor® Instrument Setup

FCS was performed on a ConfoCor®1 (Carl Zeiss, Jena, Germany). ConfoCor1 is a PC-controlled fluorescence correlation-adapted AXIOVERT 135 TV microscope equipped with an x-y-z adjustable pinhole, avalanche Photodiode SPCM-200-PQ, ALV-hardware correlator, and CCD camera. The Ar^+-laser beam (excitation wavelength 514 nm, excitation intensity 1 mW) was focused by using a water-immersion microscope objective at an open focal light cell. The same objective, a dichroic mirror, proper band-pass filters, and a pinhole in the image space block collected fluorescent light. The volume of the confocal excitation element, calibrated with AF488 or R6G, was determined to be about 1 fL (0.9 ± 0.1 fL).

Studies of DNA Binding of PicoGreen using FCS

A DNA sample for measurement (1 nM DNA, 200 μL) was loaded into one of eight-chamber cover glasses (NUNC®) with the glass bottom facing the ConfoCor water-immersion microscope objective. A small volume of PG (1:200 v/v dilution in HEPES buffer) was added stepwise into the DNA solution and the solution was incubated for 10 min before recording the fluctuation signal (30 s/time, 20 times/measurement). A calibration curve of DNA intercalation by PG was then prepared to determine the optimal dye/kbp ratio for FCS experiment.

Studies of Lipopolyamine-Mediated DNA Condensation Using FCS

A DNA sample for measurement (1 nM DNA, 200 μL) was loaded into one of eight-chamber cover glasses, followed by the addition of PG at the optimal dye/kbp ratio. After 10 min incubation, the DNA solution was titrated by DNA-condensing agents, i.e., N^4,N^9-dioleoylspermine or N^1-cholesteryl spermine carbamate. FCS reading was recorded (30 s/time, 20 times per measurement).

The composition of DNA complexes is related to the net charge of the system and expressed as N/P charge ratio (N/P = ammonium/phosphate) (40). Ammonium equivalents of the cationic component were determined from the protonation degree (from the pK_a of each amino functional group). In HEPES (pH 7.4), N^4,N^9-dioleoylspermine carries 2.0 ammonium equiv/mol (pK_a = 10.8) (41), and N^1-cholesteryl spermine carbamate (pK_a = 10.9, 8.6, 7.3) (35,36) provides 2.4 ammonium equiv/mol. The charge number was calculated by using the Henderson-Hasselbach equation. The number of phosphate equivalents was derived from the concentration of DNA measured at 260 nm.

FCS Data Analysis

FCS analysis was processed by using the ConfoCor® II software. The fluorescence intensity signal $I(t)$ fluctuating around a temporal average [$I(t) = \langle I(t)\rangle + \delta I(t)$] was processed with a digital hardware correlator interface yielding the normalized autocorrelation function or $G(\tau)$. This function is expressed as (21,42):

$$G(\tau) = \frac{\langle I(t) \times I(t+\tau)\rangle}{\langle I(t)\rangle^2} \quad (1)$$

Assuming small point-like noninteracting molecules freely diffusing in a space much larger than the detection volume, showing up only triplet state dynamics, $G(\tau)$ takes the form (21,42):

$$G(\tau) = 1 + \left(1 - T + Te^{-\tau/\tau_{tr}}\right)\left(\frac{1}{PN[1-T]}\right)\left(\frac{1}{1+(\tau/\tau_D)}\right)\left(\frac{1}{1+(\tau/\tau_D)(\omega_1/\omega_2)^2}\right)^{1/2} \quad (2)$$

where T is a triplet fraction, τ_{tr} is a triplet decay time, PN is the apparent particle number, τ_D is a diffusion time, and ω_1 and ω_2 are, respectively, the lateral and axial radii of the detection volume. The shape of the confocal volume for calculation purposes was assumed to be a cylinder (42), based on a special optical situation where the pinhole diameter and/or the objective lens were adjusted, and this volume (V) is $V = \pi\omega_1^2(2\omega_2)$. The derivation of equations for the applied models makes use of the natural laws applied in classical methods of perturbation kinetics, as the only difference is in the source of fluctuations. The parameters τ_D and PN are related with macroscopic values of concentration c, and the rate of diffusion, called the diffusion constant (43) or diffusion coefficient (D) (21) via:

$$\tau_D = \frac{\omega_1^2}{4D} \quad (3)$$

and

$$PN = cN_A\pi\omega_1^2 2\omega_2 = cN_A V \quad (4)$$

The diffusion coefficient (D) for spherically symmetric molecules is related to the hydrodynamic radius r_h via the Einstein-Stokes equation:

$$D = \frac{\omega_1^2}{4\tau_D} = \frac{k_B T_c}{6\pi\eta r_h} \quad (5)$$

where k_B is the Boltzmann constant; here T is thermodynamic temperature, η is dynamic viscosity, and r_h is hydrodynamic radius. The hydrodynamic radius can be calculated from molecular mass M using:

$$r_h = \sqrt[3]{\frac{3M}{4\pi\rho N_A}} \quad (6)$$

where ρ is the mean density of the molecule and N_A is Avogadro's number.

The translational diffusion coefficient (D) depends largely on the shape of the molecule. For rodlike molecules, such as a DNA molecule, D can be estimated as:

$$D = \frac{Ak_B T_c}{3\pi\eta L} \quad (7)$$

where L corresponds to the length of the rod [for a DNA it is the rise per base pair (0.34 nm) multiplied by the number of base pairs], d is a diameter of the rod (2.38 nm for DNA), and A represents a correction factor:

$$A = \ln(L/d) + 0.312 + 0.565/(L/d) - 0.1/(L/d)^2 \quad (8)$$

This shows that the diffusion coefficient (D) of a 1000-bp DNA is approximately five times smaller and τ_D five times larger for a rodlike-shaped molecule than for a spherical one.

RESULTS AND DISCUSSION

Measurement of the Confocal Volume in FCS

In this experiment, two fluorescent molecules, R6G (λ_{ex} = 495 nm, λ_{em} = 519 nm) and AF488 (λ_{ex} = 525 nm, λ_{em} = 555 nm) (Fig. 1) were chosen to measure the confocal volume in FCS. These fluorophores (44) have high absorption coefficients (R6G = 116,000 M^{-1} cm^{-1}, AF488 = 71,000 M^{-1} cm^{-1}) and less photobleaching, which support their use as standard dyes. The fluorescence signal from R6G or AF488 in (MilliQ) water was measured by FCS. Diffusion time (τ_D) was determined from the fluctuation caused by the diffusion of these dyes in and out of the confocal volume. Unsurprisingly, using Eq. (3), as the standard diffusion coefficient (D) of both dyes is 2.8 × 10^{-10} m^2/s, and τ_D from experiments, the excitation volume was determined to be about 1 fL (0.9 ± 0.1 fL) independently of the dye used. The dimensions of the confocal volume in our experiments are as follows: ω_1 = 0.29 ± 0.05 μm, ω_2 = 1.69 ± 0.02 μm, illustrated in Fig. 7.

Efficient Probe in DNA Condensation by FCS

EthBr fluorescence quenching assay, using a steady-state fluorimeter, has been intensively used to determine DNA

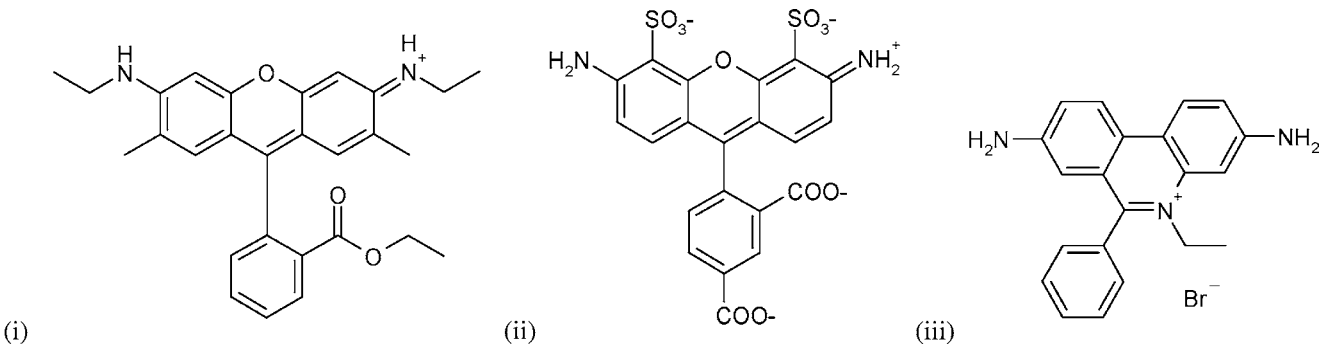

Fig. 1. Two standard fluorophores in FCS confocal volume determination: (i) R6G and (ii) AF488; (iii) EthBr is a common DNA fluorescent probe.

condensation (45). DNA intercalation with EthBr, studied using the FCS technique, was first reported by Magde's research group (46,47). The DNA-binding constant of EthBr and DNA diffusion coefficient using FCS were reported. Kral *et al.* (48,49) recently studied DNA condensation by using EthBr and propidium iodide in FCS. The count rate (CR), diffusion time (τ_D), and particle number (PN) observed by FCS at the single-molecule level, and their correlations, can be used to differentiate the nature of DNA/oligonucleotide–polycation interactions (33,43,48–50). Although EthBr is a commonly used dye in DNA-condensation studies, it was found to have effects on DNA structure at high concentration. The helical axis of DNA was dislocated by +1.0 A°, and the helix was twisted by 10°, giving rise to an angular unwinding of −26°, and the intercalated base pairs are tilted relative to one another by 8° (51). Manning's theory (12) suggested that EthBr intercalation lengthens the DNA by about 0.27 nm to the total contour length of ct DNA (52). This possible DNA conformational alteration is generally not a concern in steady-state fluorescence spectroscopy with a larger population to be measured, but this is detectable with the high sensitivity of FCS. Additionally, the higher rate of EthBr release from DNA may also lead to a significant reduction in fluorescence, making fluorescence analysis more complex. This in turn leads to the search for new fluorescent dyes that can be used without significant change in DNA conformation and also possess high absorption coefficients (which allows them to be used at low concentrations) to avoid interference in the DNA condensation behavior mediated by NVGT vectors.

Recently, a new unsymmetrical monomethine cyanine dye, PicoGreen® (PG) (Fig. 2), was introduced as a patented fluorescent dye from Roth, Haughland, and coworkers at Molecular Probes (53,54). Its chemical structure was recently reported by Zipper *et al.*, confirmed by nuclear magnetic resonance and mass spectroscopy techniques and named as [2-[*N*-bis-(3-dimethyl-aminopropyl)-amino]-4-[2,3-dihydro-3-methyl-(benzo-1,3-thiazol-2-yl)-methylidene]-1-phenyl-quinolinium]$^+$ (Fig. 2a) (37). However, this name could also be (*Chemical Abstracts* 9th CI) 2-[bis(3-dimethylaminopropyl) amino]-4-(3-methyl-2(3H)-benzothiazolylidene)methyl-1-phenyl-quinolinium (55) [178918-98-4] and/or 2-[bis-(3-di-

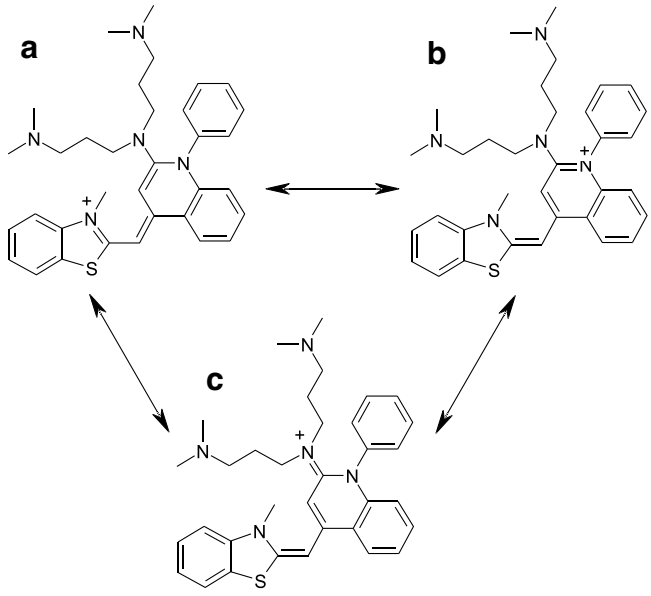

Fig. 2. PicoGreen® (PG)—an unsymmetrical monomethine cyanine dye containing a polyamine side chain to improve DNA-binding affinity with three mesomers (a, b, c).

methylaminopropyl) amino]-1-phenyl-4(1H)-quinolinylidene) methyl)-3-methyl-benzothiazolium (56) [771577-99-2]. The charge due to quaternization of the aromatic *N* atoms is delocalized, probably equally well shown residing on the *N*-methyl-benzothiazolium (Fig. 2a) (56) and on the *N*-phenyl-quinolinium (Fig. 2b) (55), in a solvent- and environment-dependent manner. There is also a contribution from the third mesomer, including the lone-pair electrons on the anilino tertiary amine, as its ammonium ion (Fig. 2c) (57).

From DNA intercalation structure–activity relationship considerations, PG carries three positive charges, i.e., one on nitrogen in the conjugated, mesomeric heteroaromatic system and two at the 3-dimethylaminopropyl residues. The cationic side chain of PG (compared to EthBr) contributes to higher affinity for double-stranded DNA (dsDNA). Biphasic mode binding was reported for PG interaction with dsDNA. Base-pair intercalation happens at low dye/base pair ratio, and external binding (minor groove) was found at higher dye/base pair ratio. At low dye/base pair ratio, PG shows no base sequence specificity. Zipper *et al.* (37) recently reported that there is no difference in binding on polydA.dT and polydG.dC, using differential absorption spectroscopy at 494 nm, if PG labeling ratio smaller than 100 dye/kbp was used. However, the fluorescence intensities of PG–DNA complexes were related to the DNA sequence at higher ratios (37). The increase in fluorescence intensity of PG upon binding to DNA is about 1000-fold (absorption coefficient 70,000 M^{-1} cm^{-1}), and this makes the background fluorescence from free dye negligible. A small red shift of the peak absorption (from 498 nm for free dye to 500 nm for the bound dye) was observed for PG (58). Interestingly, PG binds selectively to single-stranded DNA (ssDNA, low affinity) and dsDNA (high affinity) at 525 nm, unlike EthBr at 610 nm. Thus, the use of PG with EthBr simultaneously at dual wavelength (525 and 610 nm) was recently established as a novel efficient tool to determine the DNA unwinding condition (ssDNA/dsDNA ratio) (59,60). The low affinity of PG for ssDNA helps to ensure that the fluorescence detection mainly arises from dsDNA–PG interactions.

ct DNA–PicoGreen Interaction Study

Linear ct DNA has been used extensively as a model DNA for condensation studies due to its commercial availability and low cost. ct DNA is composed of a random-sequence double-stranded polynucleotide with A-T (58%) and G-C (42%) (61), which makes this DNA ideal for our studies and minimizes the effects from possible base-specific DNA-condensing agents. ct DNA is a linear DNA with minimum kbp = 13 (MW 8.580 MDa). Its contour length is 4.4 μm as calculated from the equation $L = N_{DNA} \times a$, given N_{DNA} is the average number of DNA monomer (base pairs) and a = monomer length (i.e., 0.34 nm for DNA duplex).

PG was used in our study to monitor ct DNA. PG intercalation affinity to dsDNA is higher, and it also has a higher absorption coefficient than EthBr. Fluorescence of free PG is low; thus, background fluorescence is negligible. In our experiments, fluorescence fluctuation was observed and recorded over the increase of PG concentration (i.e., labeling ratio). Experimental $G(\tau)$ functions were satisfactorily fitted to a theoretical diffusion model with a single fluorescent type. Typical normalized autocorrelation functions $G(\tau)$ are plotted as shown in Fig. 3.

The objective of the PG calibration assay is to explore the useful range of DNA labeling ratio by PG. The ideal ratio should give sufficient fluorescence signal with less interference in DNA conformation from intercalating dyes. PG, when intercalating into dsDNA, give fluorescence fluctuation signals directly recorded as "count rate" (CR). From Fig. 4(i), we see that CR increases in linear relationship with the amount of PG added, i.e., at dye molecules/kbp ratio of 5–40, and greater tolerance to the higher labeling ratio is a general trend for monointercalating dyes. Therefore, the sensitivity of the nucleic acid labeling dye to the ratio may be primarily dependent on the dissociation constant of its secondary binding mode. The higher the dye dissociation of the second binding mode, the greater the useful range of labeling ratio (compared to TOTO-1) (58). Another two parameters in FCS, diffusion time τ_D [Fig. 4(ii)] and PN [Fig. 4(iii)], remain constant as initial values at the start of experiments based on the monocomponent diffusion model. This suggests that PG has no influence over the hydrodynamic properties of DNA molecules. PG can be used at a very low level (i.e., 5–40 dye molecules/kbp), compared to a similar study using EthBr (43,48,49). The stability of PG-labeled DNA samples is also high, which means that the dilution of sample does not affect the accuracy of the measurement (58). The stability of the dye–DNA complexes after dilution is also important for a titration study of DNA condensation that involves the dilution of the sample (i.e., volume addition with DNA-condensing agent).

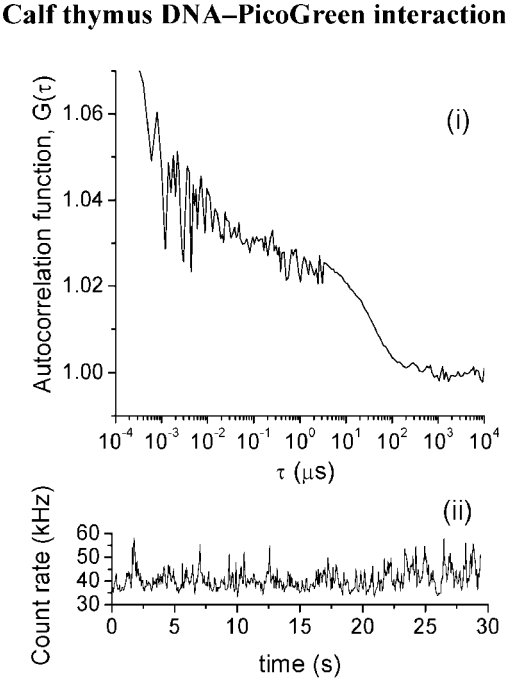

Fig. 3. Examples of (i) normalized autocorrelation function, $G(\tau)$, and (ii) the count-rate for ct DNA 1 nM (200 μL) intercalated with PG (1.1×10^{-6} M) 30 μL and $C_{dye/kbp}$ is 13. The nature of multilabeling DNA (long-chain molecules) causes an overestimation of PN (apparent PN), compared to the PN of singly labeled small molecules.

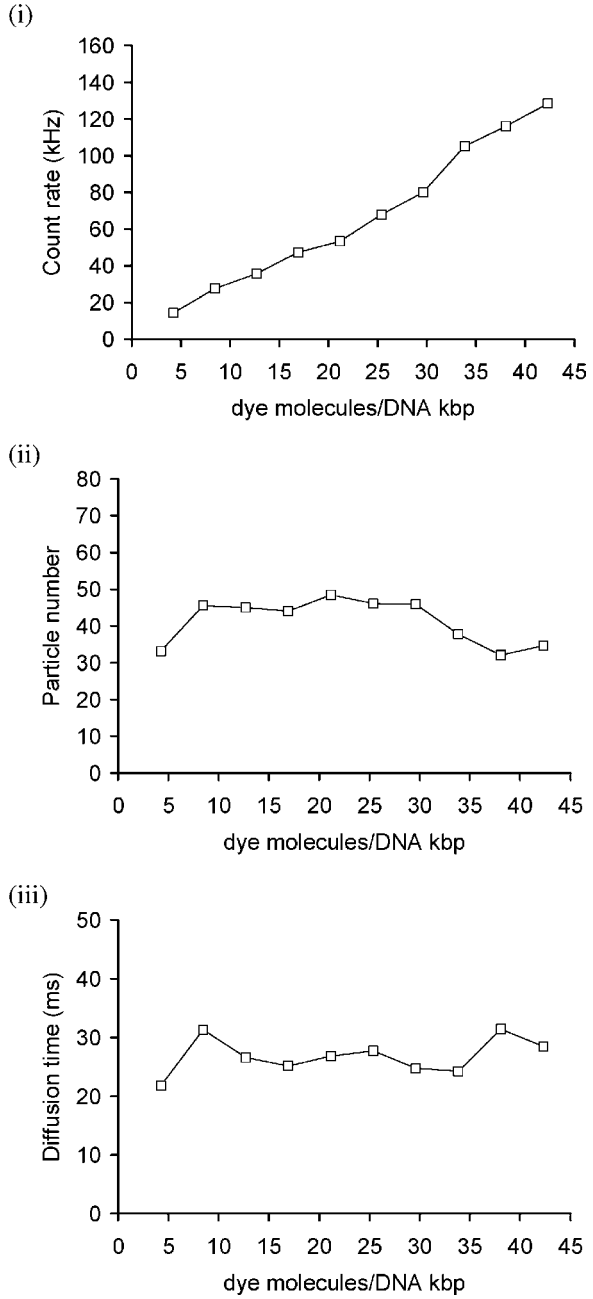

Fig. 4. PG labeling calibration using ct DNA. Different volumes of PG (1.1 μM) were added into 200 μL of 1 nM DNA and incubated for 10 min. $G(\tau)$ was recorded at each dye-labeling ratio. FCS parameters were calculated and plotted against dye concentration, i.e., (i) count rate (CR), (ii) particle number (PN), and (iii) diffusion time (τ_D).

Considering the characteristics of DNA, ct DNA has a high τ_D, which is due to its significantly greater size than circular plasmids; different-length DNAs diffuse differently in solution. The previous fluorescence recovery after photobleaching (FRAP) study using FITC-labeled DNA revealed that D_w (diffusion coefficient in water) was dependent on DNA size, $D_w = 4.9 \times 10^{-10}$ m^2/s $\times$ (bp size)$^{-0.72}$ (for 21- to 6000-bp linear dsDNA). DNA diffusion coefficient decreased by increasing DNA size indicating the complex hydrodynamic properties of DNA with respect to translational diffusion (62). Similarly, Bjorling *et al.* (63) reported that the relative translational diffusion coefficient decreased linearly with the length of dsDNA fragments (at least up to 500 bp) by using FCS in the study of DNA products formed during PCR. D_w of ct DNA from calculation (5.3×10^{-13} m^2/s) is similar to the experimental FCS result (7×10^{-13} m^2/s). Deviation of τ_D found in our FCS experiments and from calculation in ct DNA may be related to the polydispersity of ct DNA, which means that different lengths of linear DNA were measured together. However, as the DNA condensation process is regarded as an all-or-none process, it is possible to monitor the nanoparticle formation using ct DNA (64,65).

In Fig. 4(i), we see that CR increases linearly with dye concentration showing the high efficiency of PG fluorescence on DNA binding, with little effect on DNA hydrodynamic changes from the dye itself. From the labeling ratios measured and the data shown in Fig. 4, the useful concentration range of PG lies within dye molecules/kbp = 5–40, where PN is stable [Fig. 4(ii)], and there are no significant changes in diffusion time [i.e., stable conditions; Fig. 4(iii)]. In further experiments (see below), we chose a ratio of 13. FCS enables the direct measurement of the average number of fluorescent molecules (particles), the particle number (PN), diffusing through the volume element. PN was interpreted from the autocorrelation curve, described as $G(0) = 1 + (1/N)$. From Fig. 4(ii), PN calculated from $G(\tau)$ of PG molecules bound to ct DNA was 43.1 ± 8.1, which is a large overestimation of the concentration-derived theoretical PN (around 0.6 for 1 nM ct DNA). The detected fluctuations are not only due to the diffusion of the entire (multiply labeled) DNA molecules. This overestimation of PN might be due to the fact that the multiple-labeled uncondensed ct DNA (contour length = 4.4 μm) is of a size similar to the illuminated confocal element V ($2\omega_1$ = 0.58 μm, $2\omega_2$ = 3.38 μm). This leads to a high number of fluctuations in the fluorescence intensity, i.e., lower $G(\tau)$, especially when considering that the laser focus during the measurements could excite only a part of the entire chain, and thus finally lead to a higher PN. Moreover, after condensation, the DNA molecule is much smaller and the apparent PN equals the concentration-derived PN. Thus, it is clear that the overestimation of PN is due to fluctuations caused by the diffusion of parts of the DNA molecule in and out of the focus; more fluorescent events increase the apparent PN. However, from this experiment, we cannot conclude that the reason for the large PN is independent segmental motions. In our opinion, computer simulations will be needed to understand fully the physical origin of the observed high apparent PN.

ct DNA Condensation by Lipopolyamines

Two lipopolyamines were synthesized and used in these experiments. Both are designed to incorporate a spermine backbone conjugated with a lipophilic moiety, i.e., the oleoyl groups [two amide links; Fig. 5(i)] (35) and the cholesteryl group [carbamate link; Fig. 5(ii)] (36). Both our novel DNA vectors show effective condensation (i.e., yielding 90% fluorescence reduction in the EthBr fluorometric assay at N/P charge ratios as low as 1.5–2.0) and high transfection efficiency. One aim of this study is to understand more of the mechanisms by which these two vectors interact with

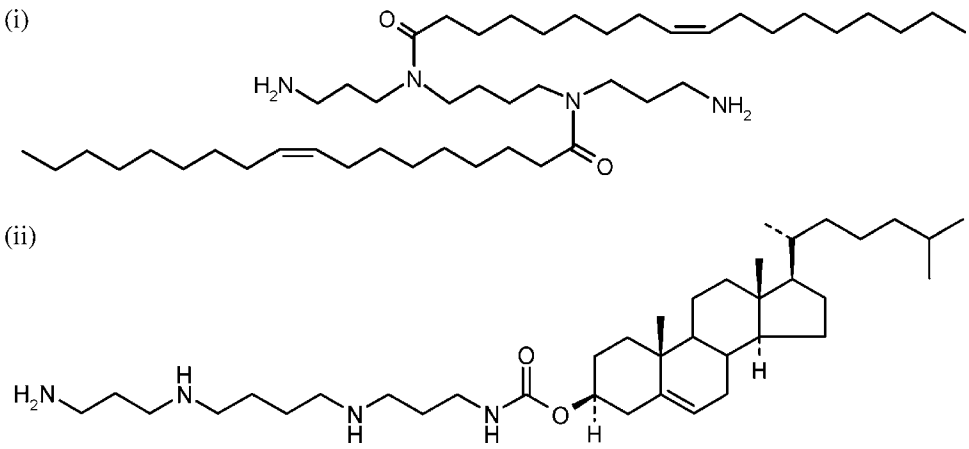

Fig. 5. (i) N^4,N^9-Dioleoylspermine, (ii) N^1-cholesteryl spermine carbamate.

DNA, as a single molecule (in this case, specifically regarded as a single nanoparticle) by FCS using PG.

From the calibration curve [Fig. 4(i)], optimal dye ratio used for ct DNA labeling was in the range of 5–40. PG was prepared in 1:200 dilution (according to the manufacturer's protocol); using too much dye would alter the total volume of sample solution. In the DNA condensation experiment, the PG volume added was 30 μL (which is equivalent to dye/kbp ratio = 13). Fluorescence fluctuation was monitored while adding N^4,N^9-dioleoylspermine and N^1-cholesteryl spermine carbamate in solution to a sample containing PG-labeled DNA.

As the N/P ratio was increased (Fig. 6), DNA phosphate groups were gradually neutralized by (positively charged) ammonium groups of N^4,N^9-dioleoylspermine and N^1-cholesteryl spermine carbamate. $G(\tau)$ was recorded and FCS parameters (diffusion coefficient and PN) were then calculated throughout the DNA condensation process. The indication of DNA condensation occurrence is the dramatic decrease of τ_D and PN particularly for a system with macromolecules where a single monitored molecule is not small enough to fit in the confocal volume. From Fig. 6, the diffusion coefficient (D) increased on the addition of lipopolyamines in both DNA condensation experiments. As faster movement of DNA resulted from condensation, we conclude that smaller (compacted) nanoparticles have been formed. PN also decreased (Fig. 6), whereas measured CR remained constant.

There are experimentally different diffusion coefficients for ct DNA molecules seen at the start of each experiment; this we assign to different lengths of ct DNA and is within experimental error. Samples of ct DNA are not by themselves homogeneous (e.g., they differ in length of nucleotide sequence); therefore, at the single molecule level, they are differently labeled by PG. This is reflected in the experimental differences recorded in the starting PN (at N/P = 0) without invalidating the use of ct DNA in such spectroscopic studies.

PN is a direct parameter to prove the number of fluorescent molecules, which here reports on the DNA concentration. In the model with point-like molecules, PN is described by the equation $PN = C \times V \times N_A$, where C = molarity of detected molecules (DNA 1 nM), V = confocal volume (1 fL), and $N_A = 6.023 \times 10^{23}$. By using this equation, and as the DNA concentrations used in our experiments were kept constant at 1 nM, the theoretical PN to be achieved is around 0.6. The PN achieved at N/P = 1.0–1.5 for ct DNA condensed by N^4,N^9-dioleoylspermine was 0.7. This evidence confirms that DNA was condensed into a point-like molecule by the C18-substituted lipopolyamine, which fulfils the assumptions of FCS and further validates the use of FCS as a sensitive method in DNA formulation studies (which is indeed a point-like molecule, when compared to the typical confocal volume, as shown in Fig. 7) (66). This result

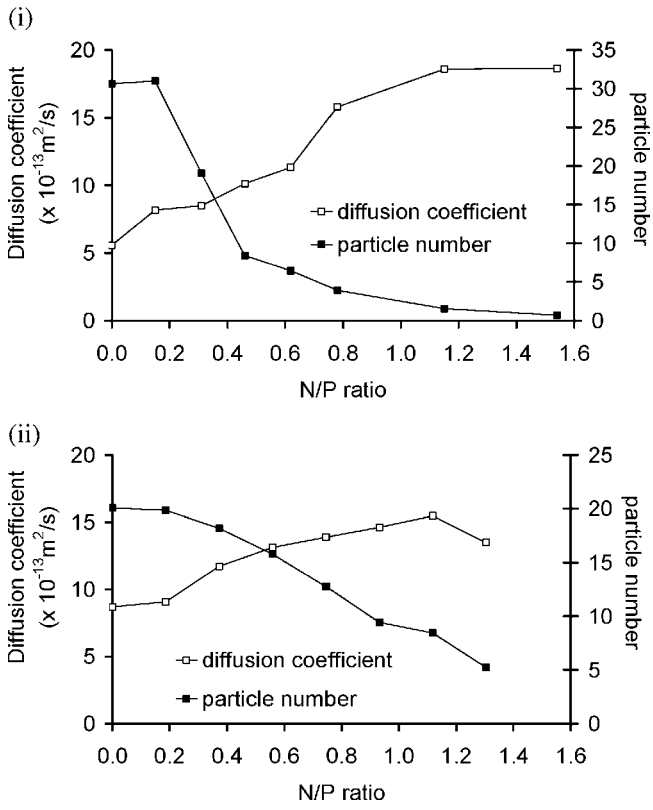

Fig. 6. FCS study of DNA nanoparticle formation: ct DNA (1 nM, 200 μL) was condensed with lipopolyamines, using PG as a reporter probe. (i) ct DNA condensation by N^4,N^9-dioleoylspermine (PG at dye/kbp = 13). (ii) ct DNA condensation by N^1-cholesteryl spermine carbamate (PG at dye/kbp = 13).

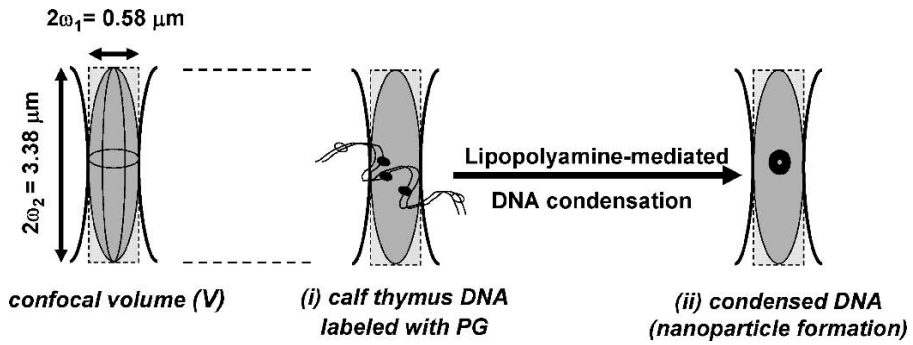

Fig. 7. DNA molecules in the FCS confocal volume (V); (i) a free (no lipopolyamine) ct DNA molecule (ribbon) labeled by intercalated PG (both open and filled circles), but only a fraction of fluorophores (filled circles) lie within the confocal volume and are therefore excited. (ii) A lipopolyamine-condensed DNA where all the PG reporter molecules now lie within the confocal volume, and all are therefore excited; this nanometer-sized complex acts as a point-like molecule (a single nanoparticle). Left, V is approximated to a cylinder of typical volume 1 fL, which is small enough to host only one particle of condensed DNA. The dimensions of the volume element were determined by using the standard fluorophores (R6G and AF488).

is in agreement with other physical studies on DNA particle size, when completely condensed at the nanoscale level (35,36).

Point-like Molecule Detection in ct DNA Condensation

Similar results were also found for DNA condensation with N^1-cholesteryl spermine carbamate—decrease in τ_D and PN. The PN value 5.2 was achieved at N/P = 1.5–2.5 for ct DNA condensed by N^1-cholesteryl spermine carbamate. From a comparison of these PN results with those obtained with N^4,N^9-dioleoylspermine, we conclude that N^1-cholesteryl spermine carbamate is a poorer DNA-condensing agent than N^4,N^9-dioleoylspermine. Additionally, condensation occurred at higher N/P ratios (N/P = 1.5–2.5) than condensation achieved with N^4,N^9-dioleoylspermine (N/P = 1.0–1.5). Considering the positive-charge number of N^4,N^9-dioleoylspermine is less than that of N^1-cholesteryl spermine carbamate (i.e., 2.0 compared to 2.4), we conclude that more efficient DNA condensation is possibly due to the respective regiochemical distribution of these two positive charges together with their lipid moieties (C18 *vs.* cholesterol).

Point-like molecules obtained from ct DNA condensation by N^4,N^9-dioleoylspermine have an average τ_D of 12.0 ms ($D = 1.8 \times 10^{-12}$ m^2/s). These nanoparticles diffuse about three times faster than free DNA ($D = 0.71 \times 10^{-12}$ m^2/s). Similar diffusion behavior of ct DNA complexed with N^1-cholesteryl spermine carbamate was also found at 14.0 ms ($D = 1.3 \times 10^{-12}$ m^2/s), although the PN has not fulfilled the point-like molecules hypothesis (i.e., not approximating to 0.6). Considering the change in the magnitude of diffusion coefficient (D) between free and condensed DNA, mediated by both our two lipopolyamines and at appropriate N/P ratios to achieve full DNA condensation, provides evidence for the dramatic change that is DNA condensation. Moreover, D is, in general for point-like molecules, a rather insensitive parameter and could incorporate some error (about 10%). On the other hand, PN is much more sensitive, and it accurately shows differences between both condensing agents. Thus, N^4,N^9-dioleoylspermine is a more efficient DNA-condensing agent (PN approaching 0.6) than N^1-cholesteryl spermine carbamate.

In conclusion, employing the reported FCS experiments, we were able to monitor lipopolyamine–DNA complex formation at the single molecule level. In comparison to other DNA markers, PG used in our FCS study has several advantages: It does not change the hydrodynamic properties of DNA, and it does not influence the lipopolyamine concentrations necessary for condensation. Additionally, due to its high brightness, PG requires 10-fold lower staining when compared with previously used markers. PG has higher affinity than EthBr and other related dyes for dsDNA, in part because of the polyamine moiety structural modification, which efficiently forms salt bridges with DNA phosphate anions; taken together with DNA intercalation, this is known as biphasic binding. Finally, count rate is practically invariant to the condensation process, indicating that dye release is not interfering with the condensation process.

As demonstrated using our lipopolyamines, FCS directly visualizes the condensation process by tracking changes in diffusion coefficients and particle numbers. In the experiments reported herein, the PN value, which is the most accurate readout parameter of an FCS experiment, gives quantitative information on the packing density of DNA–lipopolyamine aggregates. Thus, direct information on the quality of condensing molecules can be derived. This analytical platform, FCS, provides detailed information and insight about DNA and its interaction with gene carriers, which is crucial to the development of safe and effective nonviral gene delivery vectors.

ACKNOWLEDGMENTS

We thank the Universities UK for an ORS award (partial studentship support to N.A.), the Grant Agency of the Academy of the Sciences of the Czech Republic (grant A400400621 to T.K.), and the Grant Agency of the Czech Republic (GACR grant 203/05/2308 to M.H.).

REFERENCES

1. S. A. Cryan and C. M. O'Driscoll. Mechanistic studies on nonviral gene delivery to the intestine using *in vitro* differentiated cell culture models and an *in vivo* rat intestinal loop. *Pharm. Res.* **20**:569–575 (2003).
2. S. C. De Smedt, J. Demeester, and W. E. Hennink. Cationic polymer based gene delivery systems. *Pharm. Res.* **17**:113–126 (2000).
3. A. Noguchi, N. Hirashima, and M. Nakanishi. Cationic cholesterol promotes gene transfection using the nuclear localization signal in protamine. *Pharm. Res.* **19**:933–938 (2002).
4. E. Wagner, D. Curiel, and M. Cotten. Delivery of drugs, proteins and genes into cells using transferrin as a ligand for receptor-mediated endocytosis. *Adv. Drug Deliv. Rev.* **14**:113–135 (1994).
5. I. S. Blagbrough, A. J. Geall, and A. P. Neal. Polyamines and novel polyamine conjugates interact with DNA in ways that can be exploited in non-viral gene therapy. *Biochem. Soc. Trans.* **31**:397–406 (2003).
6. D. Lechardeur, A. S. Verkman, and G. L. Lukacs. Intracellular routing of plasmid DNA during non-viral gene transfer. *Adv. Drug Deliv. Rev.* **57**:755–767 (2005).
7. A. Rolland. Gene medicines: the end of the beginning? *Adv. Drug Deliv. Rev.* **57**:669–673 (2005).
8. V. A. Bloomfield. Condensation of DNA by multivalent cations—considerations on mechanism. *Biopolymers* **31**:1471–1481 (1991).
9. V.A. Bloomfield. DNA condensation by multivalent cations. *Biopolymers* **44**:269–282 (1997).
10. G. S. Manning. Limiting laws and counterion condensation in poly-electrolyte solutions. 6. Theory of the titration curve. *J. Phys. Chem.* **85**:870–877 (1981).
11. M. T. Record, C. F. Anderson, and T. M. Lohman. Thermodynamic analysis of ion effects on binding and conformational equilibria of proteins and nucleic-acids—roles of ion association or release, screening, and ion effects on water activity. *Q. Rev. Biophys.* **11**:103–178 (1978).
12. G. S. Manning. Molecular theory of polyelectrolyte solutions with applications to electrostatic properties of polynucleotides. *Q. Rev. Biophys.* **11**:179–246 (1978).
13. O. A. A. Ahmed, C. Pourzand, and I. S. Blagbrough. Varying the unsaturation in N^4,N^9-dioctadecanoyl spermines: non-viral lipopolyamine vectors for more efficient plasmid DNA formulation. *Pharm. Res.* **23**: (2006).
14. I. S. Blagbrough, N. Adjimatera, O. A. A. Ahmed, A. P. Neal and C. Pourzand. Spermine and lipopolyamines as gene delivery agents. In D. J. Beadle, I. R. Mellor, and P. N. R. Usherwood D. J. Beadle I. R. Mellor P. N. R. Usherwood (eds.), *Neurotox '03: Neurotoxicological Targets from Functional Genomics and Proteomics*, SCI, London, 2004, pp. 147–159.
15. D. McLaggan, N. Adjimatera, K. Sepčić, M. Jaspars, D. J. MacEwan, I. S. Blagbrough, and R. H. Scott. Pore forming polyalkylpyridinium salts from marine sponges *vs.* synthetic lipofection systems: distinct tools for intracellular delivery of cDNA and siRNA. *BMC Biotechnol.* **16**:6, (2006).
16. J. Zabner, A. J. Fasbender, T. Moninger, K. A. Poellinger, and M. J. Welsh. Cellular and molecular barriers to gene transfer by a cationic lipid. *J. Biol. Chem.* **270**:18997–19007 (1995).
17. W. T. Godbey, K. K. Wu, and A. G. Mikos. Tracking the intracellular path of poly(ethylenimine)/DNA complexes for gene delivery. *Proc. Natl. Acad. Sci. USA* **96**:5177–5181 (1999).
18. C. M. Wiethoff and C. R. Middaugh. Barriers to nonviral gene delivery. *J. Pharm. Sci.* **92**:203–217 (2003).
19. N. L. Thompson. Fluorescence correlation spectroscopy. In J. R. Lakowicz J. R. Lakowicz (ed)., *Topics in Fluorescence Spectroscopy*, Kluwer Academic Publishers, New York, 1991, pp. 337–378.
20. N. G. Walter, P. Schwille, and M. Eigen. Fluorescence correlation analysis of probe diffusion simplifies quantitative pathogen detection by PCR. *Proc. Natl. Acad. Sci. USA* **93**:12805–12810 (1996).
21. M. Eigen and R. Rigler. Sorting single molecules: application to diagnostics and evolutionary biotechnology. *Proc. Natl. Acad. Sci. USA* **91**:5740–5747 (1994).
22. J. Enderlein. Single molecule spectroscopy: basics and applications. In M. Hof, R. Hutterer, and V. Fidler (eds)., *Fluorescence Methods and Applications: Advanced Methods and Their Applications to Membranes, Proteins, DNA, and Cells*, Springer, Berlin Heidelberg New York, 2005, pp. 104–122.
23. N. Adjimatera, A. P. Neal, and I. S. Blagbrough. Fluorescence techniques in non-viral gene therapy. In M. Hof, R. Hutterer, and M. Hof R. Hutterer V. Fidler (eds.), *Fluorescence Spectroscopy in Biology: Advanced Methods and Their Applications to Membranes, Proteins, DNA, and Cells*, Springer, Berlin Heidelberg New York, 2005, pp. 201–228.
24. R. Brock. Fluorescence correlation spectroscopy in cell biology. In M. Hof, R. Hutterer, and V. Fidler (eds)., *Fluorescence Methods and Applications: Advanced Methods and Their Applications to Membranes, Proteins, DNA, and Cells*, Springer, Berlin Heidelberg New York, 2005, pp. 245–262.
25. R. Rigler and E. S. Elson. *Fluorescence Correlation Spectroscopy: Theory and Applications*, Springer, Berlin Heidelberg New York, 2001.
26. S. C. De Smedt, K. Remaut, B. Lucas, K. Braeckmans, N. N. Sanders, and J. Demeester. Studying biophysical barriers to DNA delivery by advanced light microscopy. *Adv. Drug Deliv. Rev.* **57**:191–210 (2005).
27. M. Gosch and R. Rigler. Fluorescence correlation spectroscopy of molecular motions and kinetics. *Adv. Drug Deliv. Rev.* **57**: 169–190 (2005).
28. N. S. White and R. J. Errington. Fluorescence techniques for drug delivery research: theory and practice. *Adv. Drug Deliv. Rev.* **57**:17–42 (2005).
29. C. Brus, E. Kleemann, A. Aigner, F. Czubayko, and T. Kissel. Stabilization of oligonucleotide–polyethylenimine complexes by freeze-drying: physicochemical and biological characterization. *J. Control. Release* **95**:119–131 (2004).
30. B. Lucas, K. Remaut, N. N. Sanders, S. C. De Smedt, and J. Demeester. Towards a better understanding of the dissociation behavior of liposome–oligonucleotide complexes in the cytosol of cells. *J. Control. Release* **103**:435–450 (2005).
31. K. Remaut, B. Lucas, K. Braeckmans, N. N. Sanders, S. C. De Smedt, and J. Demeester. FRET-FCS as a tool to evaluate the stability of oligonucleotide drugs after intracellular delivery. *J. Control. Release* **103**:259–271 (2005).
32. E. Van Rompaey, N. Sanders, S.C. De Smedt, J. Demeester, E. Van Craenenbroeck, and Y. Engelborghs. Complex formation between cationic polymethacrylates and oligonucleotides. *Macromolecules* **33**:8280–8288 (2000).
33. E. Van Rompaey, Y. Engelborghs, N. Sanders, S. C. De Smedt, and J. Demeester. Interactions between oligonucleotides and cationic polymers investigated by fluorescence correlation spectroscopy. *Pharm Res.* **18**:928–936 (2001).
34. J. Weyermann, D. Lochmann, C. Georgens, I. Rais, J. Kreuter, M. Karas, M. Wolkenhauer, and A. Zimmer. Physicochemical characterisation of cationic polybutylcyanoacrylat-nanoparticles by fluorescence correlation spectroscopy. *Eur. J. Pharm. Biopharm.* **58**:25–35 (2004).
35. O. A. A. Ahmed, N. Adjimatera, C. Pourzand, and I. S. Blagbrough. N^4,N^9-Dioleoyl spermine is a novel nonviral lipopolyamine vector for plasmid DNA formulation. *Pharm. Res.* **22**:972–980 (2005).
36. A. J. Geall, R. J. Taylor, M. E. Earll, M. A. W. Eaton, and I. S. Blagbrough. Synthesis of cholesteryl polyamine carbamates: pK_a studies and condensation of calf thymus DNA. *Bioconjug. Chem.* **11**:314–326 (2000).
37. H. Zipper, H. Brunner, J. Bernhagen, and F. Vitzthum. Investigations on DNA intercalation and surface binding by SYBR Green I, its structure determination and methodological implications. *Nucleic Acids Res.* **32**:art-e103, (2004).
38. K. L. Manchester. Value of A260/A280 ratios for measurement of purity of nucleic acids. *Biotechniques* **19**:208–210 (1995).
39. K. L. Manchester. Use of UV methods for measurement of protein and nucleic acid concentrations. *Biotechniques* **20**:968–970 (1996).
40. P. L. Felgner, Y. Barenholz, J. P. Behr, S. H. Cheng, P. Cullis, L. Huang, J. A. Jessee, L. Seymour, F. Szoka, A. R. Thierry, E. Wagner, and G. Wu. Nomenclature for synthetic gene delivery systems. *Hum. Gene Ther.* **8**:511–512 (1997).

41. J. M. Berg, J. L. Tymoczko, and L. Stryer. Protein structure and function. In *Biochemistry*, 5th ed, 2002, p.50.
42. S. T. Hess, S. H. Huang, A. A. Heikal, and W. W. Webb. Biological and chemical applications of fluorescence correlation spectroscopy: a review. *Biochemistry* **41**:697–705 (2002).
43. T. Kral, M. Hof, P. Jurkiewicz, and M. Langner. Fluorescence correlation spectroscopy (FCS) as a tool to study DNA condensation with hexadecyltrimethylammonium bromide (HTAB). *Cell Mol. Biol. Lett.* **7**:203–211 (2002).
44. N. Panchuk-Voloshina, R. P. Haugland, J. Bishop-Stewart, M. K. Bhalgat, P. J. Millard, F. Mao, W. Y. Leung, and R. P. Haugland. Alexa dyes, a series of new fluorescent dyes that yield exceptionally bright, photostable conjugates. *J. Histochem. Cytochem.* **47**:1179–1188 (1999).
45. A. J. Geall and I. S. Blagbrough. Rapid and sensitive ethidium bromide fluorescence quenching assay of polyamine conjugate–DNA interactions for the analysis of lipoplex formation in gene therapy. *J. Pharm. Biomed. Anal.* **22**:849–859 (2000).
46. D. Magde, W. W. Webb, and E. Elson. Thermodynamic fluctuations in a reacting system—measurement by fluorescence correlation spectroscopy. *Phys. Rev. Lett.* **29**:705–708 (1972).
47. D. Magde, E. L. Elson, and W. W. Webb. Fluorescence correlation spectroscopy. 2. Experimental realization. *Biopolymers* **13**:29–61 (1974).
48. T. Kral, M. Hof, and M. Langner. The effect of spermine on plasmid condensation and dye release observed by fluorescence correlation spectroscopy. *Biol. Chem.* **383**:331–335 (2002).
49. T. Kral, M. Langner, M. Benes, D. Baczynska, M. Ugorski, and M. Hof. The application of fluorescence correlation spectroscopy in detecting DNA condensation. *Biophys. Chem.* **95**:135–144 (2002).
50. P. Jurkiewicz, A. Okruszek, M. Hof, and M. Langner. Associating oligonucleotides with positively charged liposomes. *Cell Mol. Biol. Lett.* **8**:77–84 (2003).
51. H. M. Sobell, C. C. Tsai, S. C. Jain, and S. G. Gilbert. Visualization of drug–nucleic acid interactions at atomic resolution. III. Unifying structural concepts in understanding drug–DNA interactions and their broader implications in understanding protein–DNA interactions. *J. Mol. Biol.* **114**: 333–365 (1977).
52. E. Nordmeier. Absorption-spectroscopy and dynamic and static light-scattering-studies of ethidium-bromide binding to calf thymus DNA—implications for outside binding and intercalation. *J. Phys. Chem.* **96**:6045–6055 (1992).
53. P. J. Millard, B. L. Roth, H. P. T. Thi, S. T. Yue, and R. P. Haugland. Development of the FUN-1 family of fluorescent probes for vacuole labeling and viability testing of yeasts. *Appl. Environ. Microbiol.* **63**:2897–2905 (1997).
54. V. L. Singer, L. J. Jones, S. T. Yue, and R. P. Haugland. Characterization of PicoGreen reagent and development of a fluorescence-based solution assay for double-stranded DNA quantitation. *Anal. Biochem.* **249**:228–238 (1997).
55. M. Eriksson, H. J. Karlsson, G. Westman, and B. Akerman. Groove-binding unsymmetrical cyanine dyes for staining of DNA: dissociation rates in free solution and electrophoresis gels. *Nucleic Acids Res.* **31**:6235–6242 (2003).
56. J. T. Petty, J. A. Bordelon, and M. E. Robertson. Thermodynamic characterization of the association of cyanine dyes with DNA. *J. Phys. Chem. B* **104**:7221–7227 (2000).
57. H. Zipper, C. Buta, K. Lammle, H. Brunner, J. Bernhagen, and F. Vitzthum. Mechanisms underlying the impact of humic acids on DNA quantification by SYBR Green I and consequences for the analysis of soils and aquatic sediments. *Nucleic Acids Res.* **31**:art-e39, (2003).
58. X. M. Yan, W. K. Grace, T. M. Yoshida, R. C. Habbersett, N. Velappan, J. H. Jett, R. A. Keller, and B. L. Marrone. Characteristics of different nucleic acid staining dyes for DNA fragment sizing by flow cytometry. *Anal. Chem.* **71**:5470–5480 (1999).
59. L. Beach, C. Schweitzer, and J. C. Scaiano. Direct determination of single-to-double stranded DNA ratio in solution using steady-state fluorescence measurements. *Org. Biomol. Chem.* **1**:450–451 (2003).
60. C. Schweitzer and J. C. Scaiano. Selective binding and local photophysics of the fluorescent cyanine dye PicoGreen in double-stranded and single-stranded DNA. *Phys. Chem. Chem. Phys.* **5**:4911–4917 (2003).
61. H. Deng, V. A. Bloomfield, J. M. Benevides, and G. J. Thomas. Structural basis of polyamine–DNA recognition: spermidine and spermine interactions with genomic B-DNAs of different GC content probed by Raman spectroscopy. *Nucleic Acids Res.* **28**:3379–3385 (2000).
62. G. L. Lukacs, P. Haggie, O. Seksek, D. Lechardeur, N. Freedman, and A. S. Verkman. Size-dependent DNA mobility in cytoplasm and nucleus. *J. Biol. Chem.* **275**:1625–1629 (2000).
63. S. Bjorling, M. Kinjo, Z. Foldes-Papp, E. Hagman, P. Thyberg, and R. Rigler. Fluorescence correlation spectroscopy of enzymatic DNA polymerization. *Biochemistry* **37**:12971–12978 (1998).
64. G. Kleideiter and E. Nordmeier. Poly(ethylene glycol)-induced DNA condensation in aqueous/methanol containing low-molecular-weight electrolyte solutions. Part II. Comparison between experiment and theory. *Polymer.* **40**:4025–4033 (1999).
65. K. Yoshikawa, Y. Yoshikawa, and T. Kanbe. All-or-none folding transition in giant mammalian DNA. *Chem. Phys. Lett.* **354**: 354–359 (2002).
66. D. Lumma, S. Keller, T. Vilgis, and J. O. Radler. Dynamics of large semiflexible chains probed by fluorescence correlation spectroscopy. *Phys. Rev. Lett.* **90**:218301(1)–218301(4) (2003).